Article

Early-Age Properties and Reaction of Hydrophobic Portland Cement and Alkali-Activated Fly Ash–Slag Pastes with Alkyl Silanes

Rongfeng Gao [1], Jiaxi Mao [1], Shengqian Ruan [1],*, Wenlin Tu [2], Yansong Wang [3] and Dongming Yan [1],*

[1] College of Civil Engineering and Architecture, Zhejiang University, Hangzhou 310058, China
[2] Department of Engineering and Construction, University of East London, London E16 2RD, UK
[3] Department of Civil, Environmental and Geomatic Engineering, University College London, London WC1E 6BT, UK
* Correspondence: shengqian_ruan@zju.edu.cn (S.R.); dmyan@zju.edu.cn (D.Y.)

Abstract

Cementitious materials are susceptible to water ingress due to their hydrophilicity and porous microstructure, which can cause premature destruction and compromise long-term durability. Integral hydrophobic modification using alkyl silanes is an effective strategy for enhancing water resistance, while the influence of different silanes on early-age properties (within the first 7 d) of various binder systems remains unclear. This study investigates the rheology, flowability, setting behavior, reaction kinetics, compressive strength, and hydrophobicity of ordinary Portland cement (OPC) and alkali-activated fly ash–slag (AAFS) pastes incorporating alkyl silanes of varying alkyl chain lengths, i.e., methyl-(C1TMS), butyl-(C4TMS), octyl-(C8TMS), and dodecyl-trimethoxysilane (C12TMS). In OPC, C1TMS reduced yield stress and plastic viscosity by 33.6% and 21.0%, respectively, and improved flowability by 27.6%, whereas C4TMS, C8TMS, and C12TMS showed the opposite effects. In contrast, the effect of alkyl silanes on rheology and flowability of AAFS was less pronounced. Silanes delayed setting of OPC and AAFS by 5.6–164.4%, with shorter alkyl chains causing greater retardation. C1TMS and C4TMS inhibited early-age heat release and decreased the 1-day compressive strength by 14.8–35.7% in OPC and 82.0–84.5% in AAFS, whereas longer-chain silanes had comparatively minor effects. The hydrophobic performance in both binder systems was strongly correlated with alkyl chain length. C8TMS exhibited the best hydrophobicity in OPC, achieving a water contact angle of 145° and a 75.7% reduction in water sorptivity, while C4TMS demonstrated the highest hydrophobicity in AAFS. This study provides fundamental guidance for the rational selection of alkyl silanes in OPC and AAFS systems, offering insights into the design of multifunctional water-resistant cementitious composites for marine structures, building facades, and other applications with waterproofing requirements.

Keywords: fresh properties; early-age reaction; Portland cement; alkali-activated materials; hydrophobicity; alkyl silane

1. Introduction

Ordinary Portland cement (OPC), owing to its excellent mechanical performance, mature production technology, and reliable adaptability, has long been the most widely used inorganic cementitious material in civil engineering and building structures [1,2]. With the increasing demand for low-carbon and sustainable construction, alkali-activated

materials have attracted significant attention as a new generation of inorganic binders with lower energy consumption and reduced CO_2 emissions [3–5]. Clays and industrial by-products, such as metakaolin, red mud, slag, and fly ash, have shown great potential as precursors for alkali-activated materials [6–8]. Among these, alkali-activated fly ash–slag (AAFS) combines the high reactivity of slag with the favorable workability and process-ability of fly ash, exhibiting excellent mechanical properties, good formability, and efficient utilization of solid waste, making it one of the most promising systems for engineering applications [9–11].

However, both OPC and AAFS are inherently hydrophilic and porous cementitious materials. Their abundant pore structure and numerous hydrophilic hydroxyl groups make them highly susceptible to water ingress [12,13]. Water serves as the primary transport medium for aggressive ions, triggering various deterioration processes, including freeze-thaw damage, reinforcement corrosion, efflorescence, alkali-silica reaction, and sulfate or chloride attack [14–16]. Therefore, improving the water resistance of OPC and AAFS is essential for extending their service life and has been increasingly investigated in recent years [17–20].

Various strategies have been explored to enhance the water resistance of cementitious materials, including microstructural densification, pore refinement, hydrophobic modi-fication, and the construction of micro–nano hierarchical surface structures to produce lotus-leaf-like effects [21–23]. Among these, integral hydrophobic modification, which is achieved by introducing hydrophobic agents during mixing, fundamentally changes the hydrophilic nature of the cementitious matrices [24,25]. This method effectively inhibits the ingress of water and aggressive ions and improves long-term durability. Compared to surface treatments, which are prone to degradation due to wear, aging, or cracking, integral modification provides a more stable and durable hydrophobic barrier throughout the bulk material and has gained widespread interest [26–28]. A range of hydrophobic agents have been investigated, including fatty acids, polymers, fluorinated compounds, and small-molecule silanes [29–32]. Recent studies have also demonstrated that incorpo-rating nanomaterials such as nanoclay into cementitious materials can effectively reduce water absorption and sorptivity [33,34]. Among them, small-molecule silanes, particularly alkyl silanes, have attracted increasing attention owing to their unique chemical reactivity and excellent hydrophobicity [35,36]. Alkyl silanes typically possess a general structure of $(RO)_3–Si–X$ and can hydrolyze in moist conditions to form silanols (Si–OH), which subsequently condense into silica gels or react with hydroxyl groups in OPC or AAFS matrix to form stable Si–O–Si bonds [37,38]. The functional group –X plays a crucial role, with alkyl groups being among the most effective functionalities for hydrophobic enhance-ment [39,40]. Recent studies have demonstrated that alkyl silanes can substantially improve hydrophobicity in both OPC and AAFS pastes when integrally incorporated [41–45]. It was found that the water absorption in cement pastes was reduced by up to 70% with the addition of 0.8% isooctyl-triethoxysilane [41]. A water contact angle (WCA) of 108° in lightweight concrete modified with 4% isobutyl-triethoxysilane was achieved by the previous study, which increased to 159° when 2% nano-SiO_2 was added to create a uniform microporous structure and hierarchical surface roughness [42]. Similarly, She et al. found that incorporating 0.5–2% isooctyl-triethoxysilane reduced the water absorption of AAFS by over 50%, with a maximum WCA of 118° [45].

Nevertheless, the hydrolysis, condensation, and organic–inorganic hybridization of alkyl silanes can interfere with the dissolution, hydration, gelation, and polymerization processes of OPC or AAFS, thereby affecting their early-age fresh and mechanical properties such as rheology, flowability, setting time, and compressive strength [45–49]. For example, Yang et al. investigated the effects of hydrophobic isobutyl-triethoxysilane on OPC hydra-

tion and observed that although it had little influence on the initial dissolution of cement particles, it markedly retarded subsequent hydration reactions [46]. Koohestani reported that adding 1% methyl-trimethoxysilane in cement–tailing mixtures reduced the water demand by up to 25% at a constant slump height, indicating improved dispersion of the mixture [47]. Furthermore, it was found that incorporating 0.5% dodecyl-triethoxysilane had negligible effects on setting time but significantly increased the apparent viscosity of OPC pastes [49]. She et al. reported that isooctyl-triethoxysilane accelerated the early reaction of AAFS pastes within the first 72 h and enhanced their 1-day compressive strength [45]. These findings highlight that alkyl chain length plays a critical role in determining the impact of silanes on the fresh-state behavior and early reactivity of cementitious systems. Longer alkyl chains generally provide lower surface energy and higher hydrophobicity, but they may also exhibit reduced solubility, increased steric hindrance, and self-condensation, resulting in complex and unpredictable effects in inorganic systems [50,51]. Moreover, the distinct chemical environments, particle interactions, and reaction mechanisms in OPC and AAFS may lead to markedly different behaviors of alkyl silanes in these two systems. Despite the growing interest in silane-based hydrophobic modification, most existing studies have focused on a single type of alkyl silane, evaluating its effects on one specific binder system, most commonly on OPC. These investigations have predominantly emphasized long-term performance indicators, such as surface hydrophobicity, capillary water absorption, pore structure refinement, and compressive strength development. However, the early-age performance of different types of alkyl silane across comparative binder systems has barely been comprehensively studied. Although a few studies have considered early hydration processes, there remains a lack of systematic research on how alkyl silanes with varying chain lengths regulate early-age properties in both OPC and AAFS systems [21]. Considering that early-age properties directly influence the workability, initial structural stability, and subsequent pore densification of cementitious materials, it is vital to conduct this study for the development of water-resistant cementitious materials and their further practical application.

To address the research gap, this study systematically investigates the effects of four representative silanes with different alkyl chain lengths: methyl-trimethoxysilane (C1TMS), butyl-trimethoxysilane (C4TMS), octyl-trimethoxysilane (C8TMS), and dodecyl-trimethoxysilane (C12TMS). These four silanes were chosen to represent a progressive range from short to long alkyl chains, enabling systematic evaluation of how chain length affects early-age properties and reactions of OPC and AAFS pastes. It is hypothesized that increasing the alkyl chain length of silanes will enhance hydrophobicity but may reduce workability and alter early-age reaction behavior, with these effects differing between OPC and AAFS systems due to their distinct chemistries. Early-age properties, such as rheology, flowability, and setting time, as well as early reaction kinetics, compressive strength, and hydrophobicity were comprehensively evaluated to elucidate the chain-length-dependent regulatory mechanisms and organic–inorganic hybridization behaviors in these two systems. The findings aim to provide a reference for the rational selection of alkyl silanes in different cementitious systems and offer new insights into the design and optimization of multifunctional water-resistant cementitious materials.

2. Experimental Program

2.1. Raw Materials

OPC clinker of P.O. 42.5 grade was used to prepare the cement-based paste samples. Low-calcium fly ash (FA) and ground granulated blast-furnace slag (GGBS) were used as precursors for the AAFS paste samples. The chemical compositions, which were measured by X-ray fluorescence spectrometry (XRF), are presented in Table 1. The morphologies

observed using a scanning electron microscope and particle size distributions of OPC, FA, and GGBS are presented in Figure 1. The median particle size Dv (50) of the OPC used in this study was 17.97 μm, and those of FA and GGBS grains were 12.19 μm and 12.51 μm, respectively. The alkaline activator solution for preparing AAFS was composed of sodium silicate solution (SS, pH = 10.4, SiO_2 = 26.77 wt.%, Na_2O = 8.32 wt.%, Hengli Chem. Co., Ltd., Jiaxing, China) and sodium hydroxide pellets (SH, purity: ≥96%, Sinopharm Chemical Reagent Co., Ltd., Shanghai, China). Four types of silanes with progressively increasing alkyl chain length, including C1TMS, C4TMS, C8TMS, and C12TMS, were selected as hydrophobic modifiers. These alkyl silanes were supplied by Bide Pharmatech Ltd., Shanghai, China, with molecular formulas and structures listed in Table 2. All the alkyl silanes were colorless and transparent liquids with a purity of 95–98%, as verified by the supplier using GC, HPLC, and NMR. They were stored in airtight amber glass bottles, under dry conditions at 20 ± 2 °C, and away from direct sunlight until use.

Table 1. Chemical composition of OPC, FA and GGBS (wt.%).

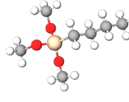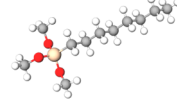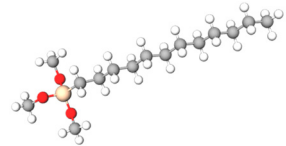| Oxide	SiO_2	Al_2O_3	CaO	Fe_2O_3	TiO_2	Na_2O	K_2O	MgO	P_2O_5	SO_3	MnO
OPC	22.27	6.34	56.08	4.51	0.59	0.57	1.10	3.91	0.18	4.11	0.22
FA	51.21	28.28	4.23	5.38	1.07	0.53	1.28	0.82	0.19	0.47	0.05
GGBS	28.12	14.28	44.8	0.35	0.74	0.29	0.29	7.58	0.02	1.65	0.14
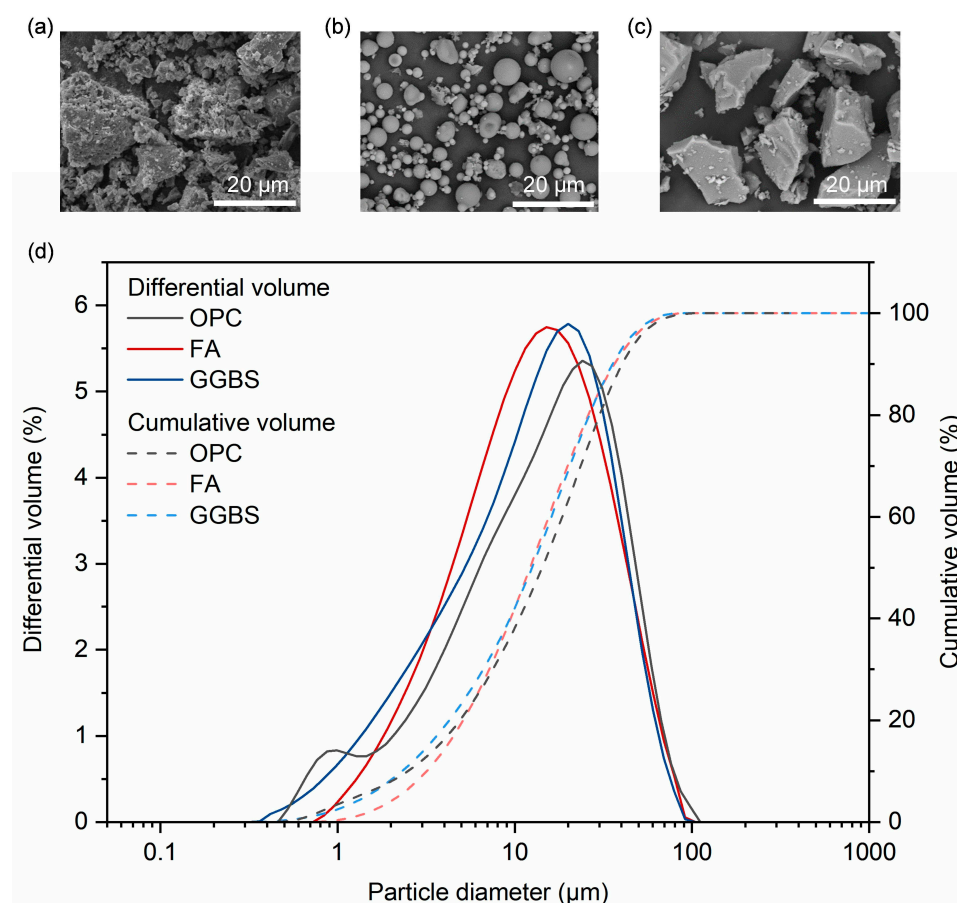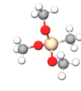
Figure 1. Morphology of (**a**) OPC, (**b**) FA, and (**c**) GGBS, and their (**d**) particle size distribution.

Table 2. Chemical information on alkyl silanes used in this work.

Alkyl Silane	Abbreviation	Molecular Formula	Molecular Structure
Methyl-trimethoxysilane	C1TMS	$C_4H_{12}O_3Si$	
Butyl-trimethoxysilane	C4TMS	$C_7H_{18}O_3Si$	
Octyl-trimethoxysilane	C8TMS	$C_{11}H_{26}O_3Si$	
Dodecyl-trimethoxysilane	C12TMS	$C_{15}H_{34}O_3Si$	

2.2. Sample Preparation

The basic mix proportions of the OPC and AAFS pastes are summarized in Table 3. Based on previous studies on organic–inorganic hybrid cement and AAFS systems, the alkyl silane dose (mass ratio to the paste) was set as 1%, which has been reported to achieve good hydrophobic modification effects [29,32,45,52]. All OPC pastes were prepared with a water-to-cement ratio of 0.45 to ensure proper emulsification and hydrolysis of silanes. The AAFS pastes were prepared with the same water-to-solid ratio of 0.45. The water in the AAFS system was from SS solution and additional water, and the solid part comprised FA and GGBS. The reference OPC and AAFS pastes without silanes were designated as OPC_Ref. and AAFS_Ref., respectively. The silane-modified pastes were labeled as OPC_C*n* and AAFS_C*n*, where *n* = 1, 4, 8, and 12 correspond to the incorporation of C1TMS, C4TMS, C8TMS, and C12TMS, respectively.

Table 3. Mix proportions of OPC and AAFS pastes (g).

Specimen Designation	OPC	FA	GGBS	Water	SS Solution	SH	Alkyl Silanes
OPC_Ref.	100	-	-	45	-	-	0
OPC_C*n*	100	-	-	45	-	-	1.45
AAFS_Ref.	-	50	50	21.3	36.5	2.6	0
AAFS_C*n*	-	50	50	21.3	36.5	2.6	1.60

Figure 2 shows the preparation process and test methods for OPC and AAFS pastes. For OPC pastes, the silane emulsions were prepared by adding the required amount of silane into deionized water using a pipette, followed by mechanical emulsification with an electric mixer at 1200 r/min for 10 min. The emulsions were then allowed to rest for 5 min to remove air bubbles. Cement was subsequently mixed with the silane emulsion (or deionized water for the reference samples) to produce fresh OPC pastes, following a two-step procedure: low-speed mixing (140 ± 5 r/min) for 2 min for initial blending, then high-speed mixing (285 ± 10 r/min) for 3 min to ensure homogeneity. For AAFS pastes, the alkaline activator solution was prepared 24 h in advance by mixing SS solution, deionized water, and SH. The mixture was then sealed and allowed to cool to achieve a clear state. The silane emulsion was produced by combining the designated amount of silane with the prepared alkaline activator solution, followed by emulsification at 1200 r/min for 10 min

and 5 min standing to release air bubbles. Meanwhile, FA and GGBS solids were thoroughly premixed to ensure homogeneity. The fresh AAFS pastes were then obtained by mixing FA, GGBS, and the silane emulsion using the same mixing protocol as for OPC pastes. For the reference group, a silane-free alkaline activator solution was used. The macroscopic appearance and binarized microscopic images of emulsions after 5 min of resting following mechanical emulsification are shown in Figure 3. The results indicate that, prior to mixing with FA, GGBS, or cement, the silanes were uniformly dispersed in the emulsions as small oil droplets (5–80 µm), showing good stability in both deionized water and alkali activator solution. Fresh OPC and AAFS pastes were subsequently tested for flowability, rheology, and setting time. For reaction kinetics tests, pastes were prepared separately as detailed in the corresponding section. For compressive strength, water contact angle, and water absorption tests, the pastes were cast into molds, sealed with plastic film, and cured in a standard curing room (RH > 95%, 25 ± 2 °C). After 24 h, samples were demolded; a portion was tested for 1-day compressive strength, while the remaining specimens were continuously cured under the same conditions until the specified test ages.
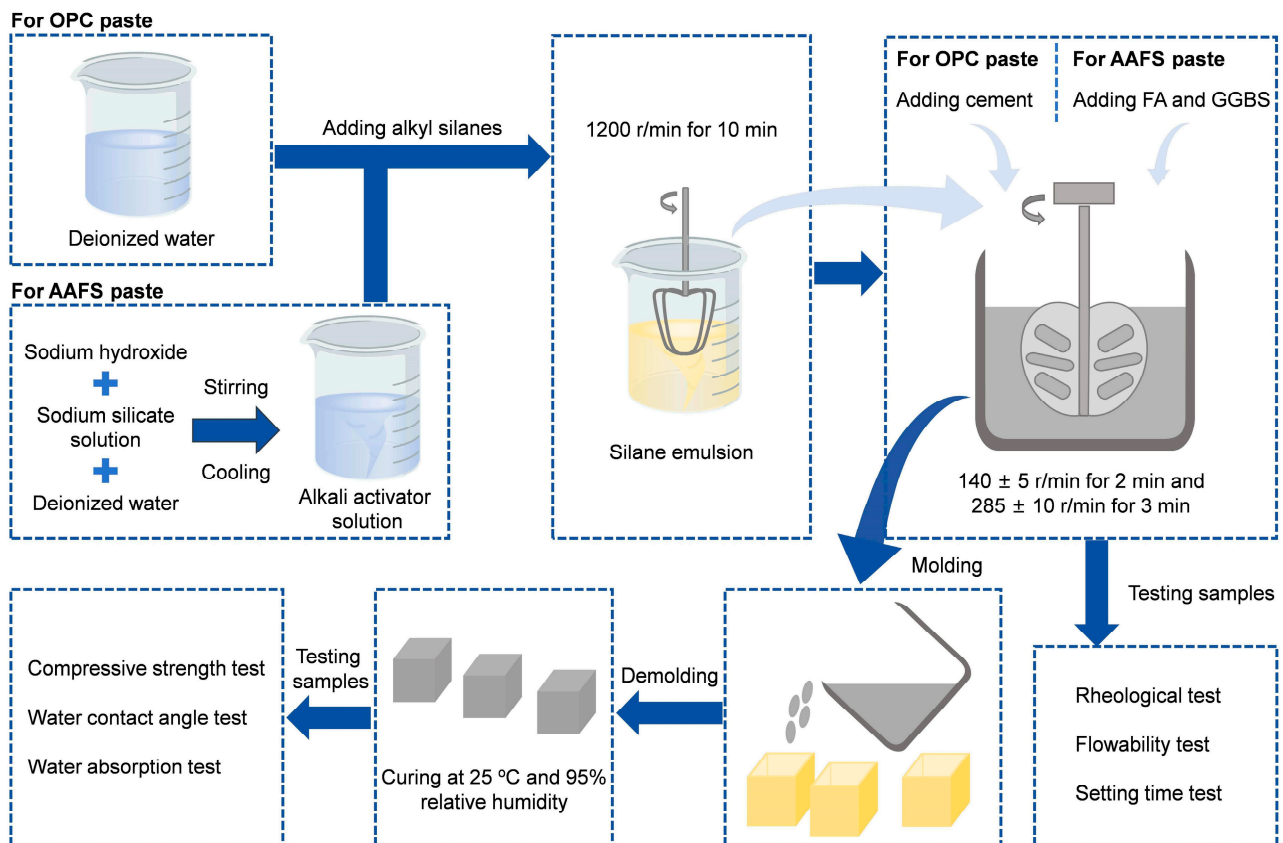

Figure 2. Schematic diagram of preparation procedure and test methods for OPC and AAFS pastes.
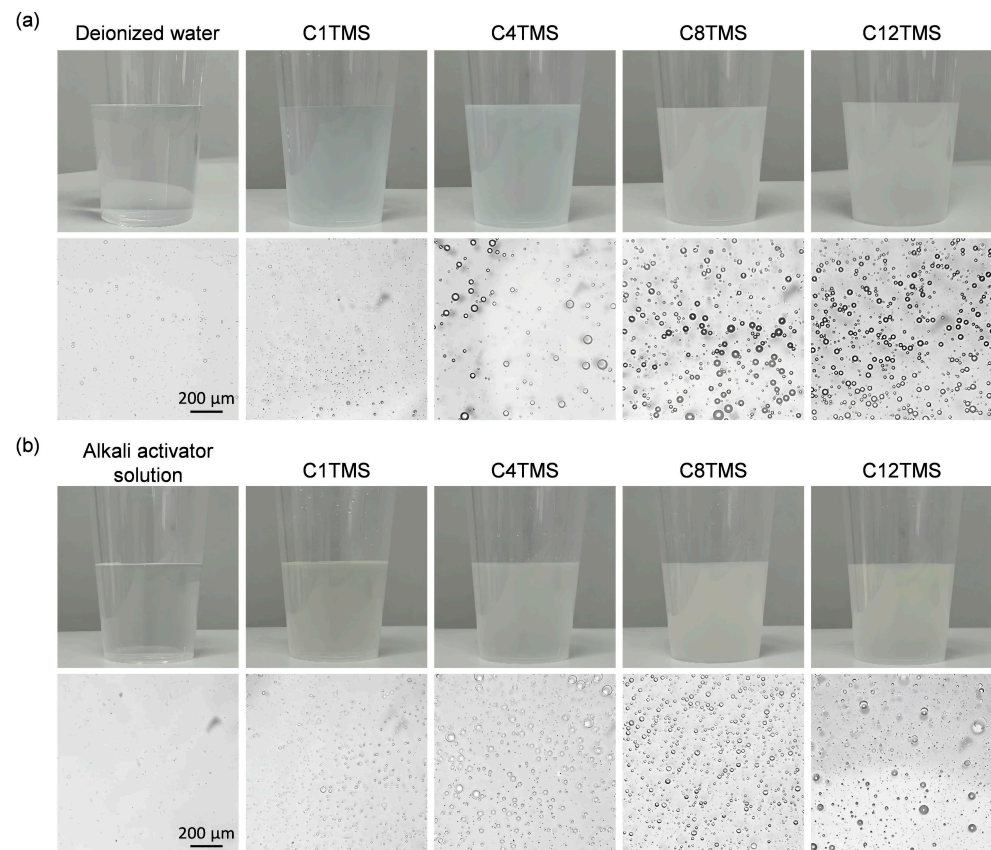
Figure 3. Macroscopic appearance and binarized microscopic images of emulsions after 5 min of resting following mechanical emulsification: (**a**) emulsions prepared in deionized water (silane-to-water mass ratio = 1.45:45); (**b**) emulsions in alkali activator solution (silane-to-activator solution mass ratio = 1.60:60.4).

2.3. Testing Methods

2.3.1. Rheological Test

The rheological properties of the fresh OPC and AAFS pastes were measured 10 min after the start of mixing, which included 5 min of mixing followed by a 5 min resting period for sample transfer and instrument preparation. All mixtures were subjected to the same procedure to ensure comparability. Rheological measurements were performed using a Viscotester IQ AIR rheometer (Thermo Fisher Scientific Inc., Waltham, MA, USA) in a controlled environment at 20 ± 1 °C and $55 \pm 5\%$ relative humidity, and the testing equipment and procedure are shown in Figure 4. The loading program consisted of two stages [53]. In the pre-shearing stage, pastes were pre-sheared at a constant shear rate of $100 \ \text{s}^{-1}$ for 60 s to minimize the influence of any structural build-up during resting. In the testing stage, the shear rate was linearly increased from 0 to $100 \ \text{s}^{-1}$ within 100 s, followed by a decrease back to $0 \ \text{s}^{-1}$ over the next 100 s. Each test was performed in triplicate using independently prepared fresh pastes. A representative curve providing the closest result to the average of the three tests is presented for each mixture [54]. The dynamic yield stress and plastic viscosity were determined by analyzing the part of the descending curve [55,56].
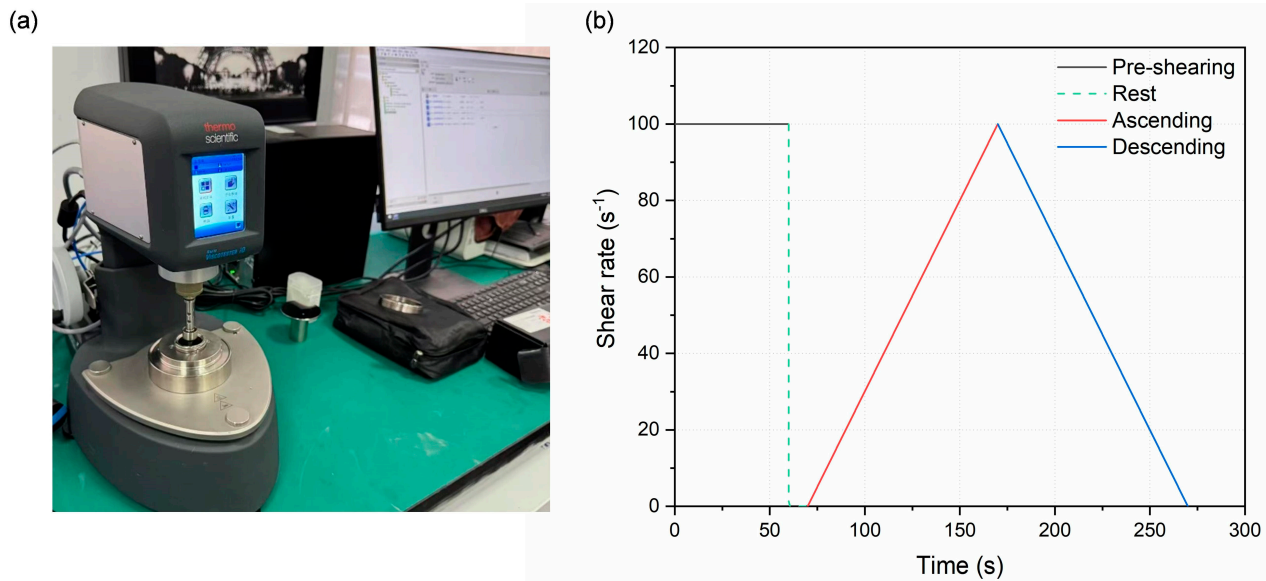
Figure 4. (**a**) Equipment for testing and (**b**) schematic representation of applied rheology protocol.

2.3.2. Flowability Test

Referring to GB/T 8077-2023 [57], the flowability of fresh OPC and AAFS pastes was characterized by the average of the free spreading diameters measured in two mutually perpendicular directions on a smooth glass plate [58]. After mixing for 5 min, the paste was rapidly poured into a hollow truncated cone (36 mm × 60 mm × 60 mm). The cone was then vertically and swiftly lifted, allowing the paste to spread freely on the glass plate. The final flow diameter was recorded exactly 30 s after lifting the cone. Each set of tests was performed twice, and the average was taken if the difference between the two values was less than 5 mm; if the difference exceeded 5 mm, a third measurement was conducted, and the average of the two closest values was reported.

2.3.3. Setting Time Test

The setting times were determined according to GB/T 1346-2024 [59] using a Vicat apparatus (Shangyu Exploration Instrument Factory, Shaoxing, China) under controlled conditions of 20 ± 2 °C and relative humidity ≥ 95%. Freshly prepared paste was immediately poured into a standard Vicat mold (40 mm × 65 mm × 75 mm) placed on a clean glass plate. During the test, the mold and the glass plate were positioned beneath the plunger of the Vicat apparatus, and the standard needle was brought into gentle contact with the surface of the paste and allowed to penetrate freely under its own weight. The initial setting time was defined as the time when the initial setting needle reached a penetration depth of 4 ± 1 mm from the base plate. The final setting time was defined as the time when the annular attachment of the final setting needle no longer left any visible mark on the paste surface.

2.3.4. Reaction Kinetic Test

Isothermal calorimetry was performed to examine the effect of alkyl silanes on early-age reaction kinetics. The tests were conducted using a calibrated CHH-CAL isothermal calorimeter (Beijing Hongruijia Technology Co., Ltd., Beijing, China) at a constant temperature of 20 °C. For OPC pastes, 3.0 g of cement and the corresponding mass of the pre-prepared silane emulsion (or deionized water for the reference group) were added to glass ampules. For AAFS pastes, 1.5 g of FA and 1.5 g of GGBS were combined with the corresponding mass of silane emulsion (or silane-free solution for the reference group) in the ampules. Each ampule was immediately mounted on a vortex mixer and homogenized

for 60 s at 1500 rpm to ensure uniform dispersion. The ampules were transferred into the calorimeter chamber within 15 s of mixing completion. Heat flow and cumulative heat release were continuously recorded for up to 88 h. Both heat flow and cumulative heat release values were normalized by the binder mass and expressed as heat release per gram of binder.

2.3.5. Compressive Strength Test

The compressive strength of 1, 3, 7, and 28-day cured pastes was determined using an LCY-300DF testing machine (Zhejiang Lizheng Instrument Equipment Co., Ltd., Hangzhou, China), referring to GB/T 17671-2021 [60]. Each reported value is the mean of six specimens, and the loading process was ensured to be quasi-static, with a loading speed of 2.4 kN/s.

2.3.6. Water Contact Angle Test

The static WCA was measured using a DropMeter A-100P instrument (Ningbo Haishu Maishi Testing Technology Co., Ltd., Ningbo, China) by placing approximately 5 μL water droplets on the polished fracture surfaces of pastes cured for 28 d. Surface roughness may influence WCA measurements by altering the solid–liquid contact area or introducing air–liquid interfaces. To minimize the influence of surface roughness, the fracture surfaces were sequentially polished using 120-, 400-, and 800-mesh sandpapers for a total of 10 min, ensuring comparable micron-scale roughness across all specimens [61]. Prior to testing, all pastes were dried at 60 °C for 8 h. For each sample, five droplets were tested at different positions along the central area of the polished surface, avoiding visible pores or defects. The reported WCA value represents the average of these five measurements.

2.3.7. Water Absorption Test

Referring to ASTM C642-13 [62], the water adsorption characteristics were assessed on 28-day cured cubic paste samples (40 mm per side). Capillary absorption is the dominant behavior of water transport in unsaturated porous materials and is typically studied under unidirectional conditions [63]. Before testing, pastes were dried at 60 °C for 48 h, and then all surfaces except the water absorption side were sealed with epoxy resin. The pastes were subsequently immersed in water to a depth of approximately 3 mm, and the mass gain was recorded at regular intervals.

3. Results and Discussion

3.1. Rheology

Rheology is a typical indicator for evaluating the workability of fresh cementitious materials. Figure 5 illustrates the shear stress and apparent viscosity of fresh OPC and AAFS pastes incorporating 1% alkyl silanes. All pastes exhibited a linear relationship between shear stress and shear rate, indicating Bingham fluid behavior [64]. The relationship between shear stress and shear rate for all mixtures was fitted using the Bingham model, and the dynamic yield stress and plastic viscosity were determined according to Equation (1) [54,64]:

$$\tau = \tau_0 + \mu_P \gamma \tag{1}$$

where τ is the shear stress (Pa), τ_0 is the yield stress (Pa), μ_p is the plastic viscosity (Pa·s), and γ is the shear rate (s^{-1}).
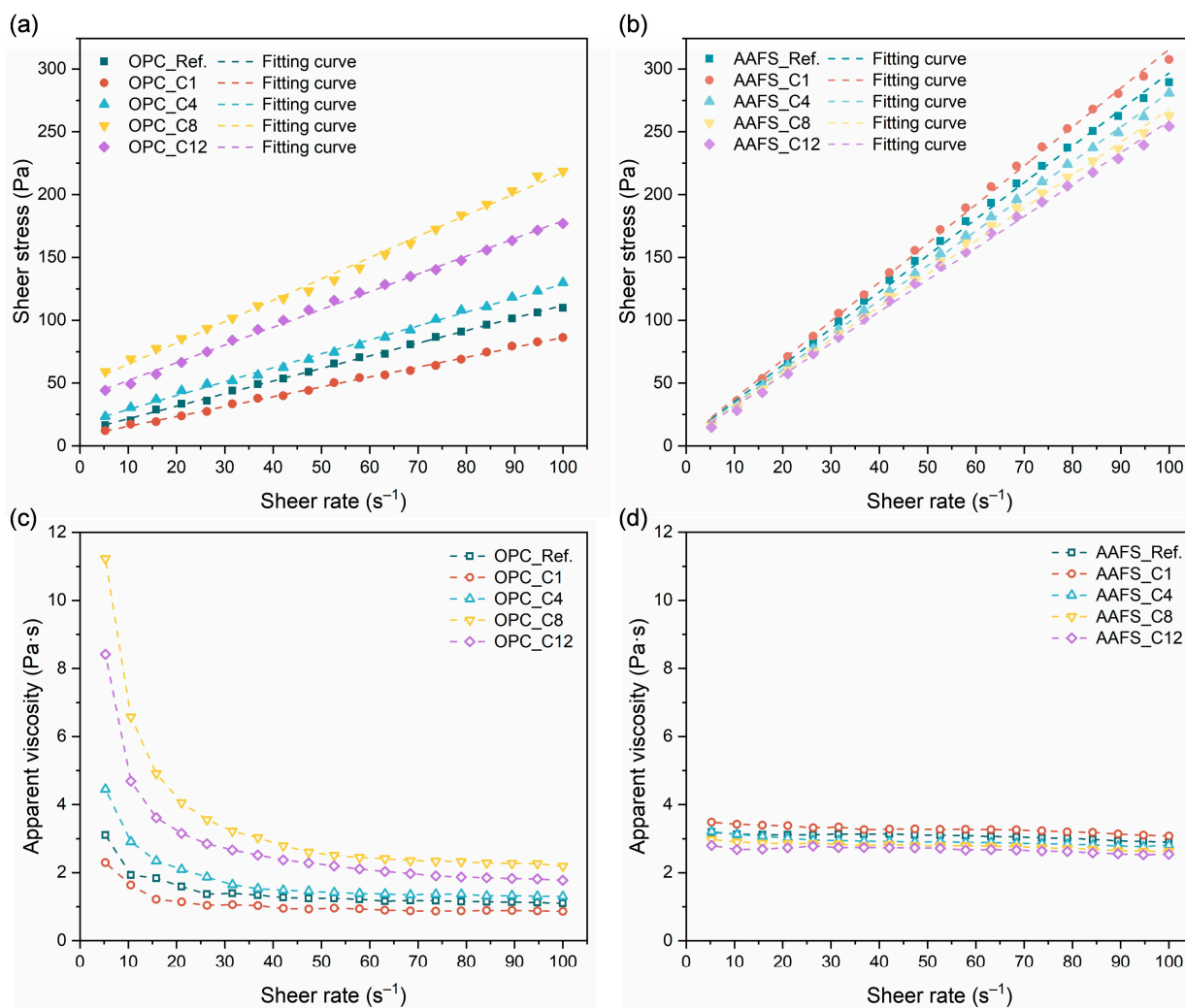
Figure 5. Rheological curves of fresh (**a**,**c**) OPC and (**b**,**d**) AAFS pastes with 1% alkyl silanes: (**a**,**b**) shear stress and (**c**,**d**) apparent viscosity.

Table 4 presents the fitted yield stress and plastic viscosity, showing excellent agreement with the Bingham model (Equation (1), $R^2 > 0.99$ for all tests). The yield stress primarily reflects colloidal interactions among particles, whereas the plastic viscosity characterizes flow resistance caused by internal flocculation or network structuring [65,66]. For the reference OPC paste, the yield stress and plastic viscosity were 11.60 Pa and 1.00 Pa·s, respectively. The addition of C1TMS significantly reduced both parameters, with yield stress decreasing by 33.6% and plastic viscosity decreasing by 21.0% for the OPC system. This behavior can be attributed to the short-chain molecular structure of C1TMS, which enables rapid hydrolysis to generate highly hydrophilic methylsilanol species. Benefiting from its excellent dispersion in the aqueous phase, C1TMS readily condenses with hydroxyl groups in the cement matrix, reducing interparticle flocculation and bridging interactions, thereby enhancing particle dispersion and lowering the flow resistance of the fresh paste [67,68]. In contrast, the viscosity results for the samples with C4TMS, C8TMS, and C12TMS all significantly increased. Specifically, C4TMS increased yield stress and plastic viscosity by 54.2% and 11.0%, respectively. C8TMS showed the highest increase (314.6% and 70.0%, respectively), while C12TMS induced slightly lower increments (227.0% and 41.0%). This enhancement mainly arises from the stronger hydrophobicity of medium-to long-chain silanes, which tend to self-aggregate and adsorb onto particle surfaces, form-

ing hydrophobic clusters. These clusters reduce cement particle wettability, increase steric hindrance, and promote network formation, thereby raising the initial viscosity [50,69].

Table 4. Yield stress and plastic viscosity of all mixtures using the Bingham model.

Mixture	Yield Stress	Plastic Viscosity	Mixture	Yield Stress	Plastic Viscosity
	τ_0 (Pa)	μ_p (Pa·s)		τ_0 (Pa)	μ_p (Pa·s)
OPC_Ref.	11.60	1.00	AAFS_Ref.	6.25	2.91
OPC_C1	7.70	0.79	AAFS_C1	6.68	3.09
OPC_C4	17.89	1.11	AAFS_C4	5.61	2.76
OPC_C8	48.09	1.70	AAFS_C8	6.08	2.62
OPC_C12	37.93	1.41	AAFS_C12	5.74	2.53

Compared with OPC, the changes in shear stress and apparent viscosity of AAFS pastes after alkyl silane incorporation were relatively small, showing a distinct behavior as seen in Figure 5b,d. The AAFS reference paste exhibited a much higher plastic viscosity (2.91 Pa·s, approximately three times that of OPC), mainly attributed to the higher viscosity of the alkaline activator compared to water [65,70]. This inherently high viscosity likely limited the ability of 1% alkyl silane to significantly alter the overall rheological properties. Specifically, C1TMS slightly increased the yield stress and plastic viscosity of AAFS to 6.68 Pa and 3.09 Pa·s (6.8% and 6.2% increase, respectively). This can be explained by the rapid hydrolysis of C1TMS in the highly alkaline environment, generating large amounts of methylsilanol that condense with reactive Si–OH and Al–OH groups to form localized cross-linked networks, thereby slightly enhancing structural cohesion. In contrast, C4TMS, C8TMS, and C12TMS slightly reduced yield stress (by 2.7–10.2%) and plastic viscosity (by 5.2–13.1%). Because medium- and long-chain silanes hydrolyze more slowly, their hydrophobic chains may preferentially adsorb onto particle surfaces, forming localized hydrophobic coatings that reduce direct particle contact. Meanwhile, dispersed hydrophobic chains in the pore solution may act as lubricants, creating slip interfaces between particles and lowering internal friction. Overall, the chain-length effect of silanes is highly dependent on the chemical environment. Short-chain silanes markedly reduce viscosity in OPC pastes due to improved particle dispersion, but may slightly increase viscosity in AAFS pastes by promoting localized gel formation and particle bridging. Medium- and long-chain silanes significantly increase viscosity in OPC by reducing local wettability and increasing steric hindrance, whereas in the more viscous AAFS system, they tend to slightly reduce viscosity by weakening direct particle contacts and providing lubrication [49].

3.2. Flowability

The effects of alkyl silanes on the flow diameters of fresh OPC and AAFS pastes are shown in Figure 6. It is noteworthy that, at the same water-to-binder ratio of 0.45, the AAFS paste showed better flowability than the OPC paste. Although AAFS pastes exhibited higher overall plastic viscosity, their lower yield stress, combined with the "ball-bearing" effect of FA particles that reduced interparticle friction, resulted in lower apparent viscosity at low shear rates and easier flow initiation [71]. C1TMS increased the flowability of OPC pastes by 27.6%, consistent with its viscosity-reducing effect observed in rheological tests. In contrast, C4TMS, C8TMS, and C12TMS decreased OPC paste fluidity by 6.7%, 35.7%, and 30.3%, respectively, primarily because hydrophobic chains increase steric hindrance between cement particles and restrict slurry flow. In AAFS pastes, the effects of alkyl silanes were relatively small: C1TMS slightly reduced flowability to 204.25 mm (3.1% reduction), while C4TMS, C8TMS, and C12TMS increased flowability

by 3.3–7.0%. These results indicate that alkyl silanes have limited ability to substantially restructure interparticle interactions in AAFS; medium- and long-chain alkyl silanes mainly act by forming hydrophobic coatings and providing localized lubrication, slightly reducing particle contacts but with limited overall improvement in flowability.
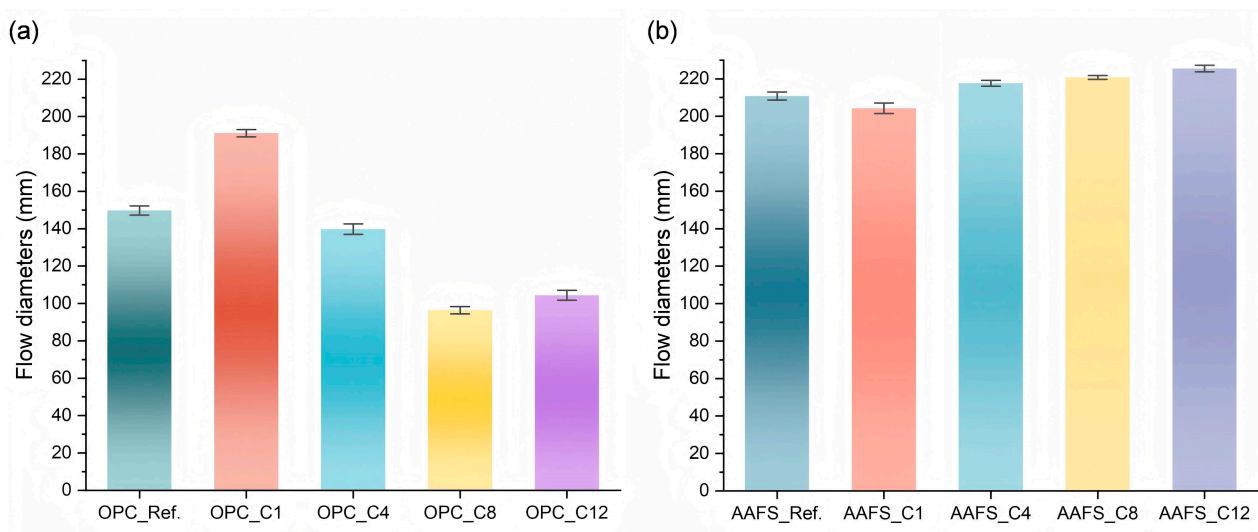

Figure 6. Flow diameters of fresh (**a**) OPC and (**b**) AAFS pastes with 1% alkyl silanes.

3.3. Setting Time

Figure 7 presents the initial and final setting times of OPC and AAFS pastes with 1% alkyl silanes. All silanes delayed OPC paste setting, with the retardation effect decreasing as chain length increased, consistent with previous findings [48]. C1TMS extended the final setting time by 164.4%. This was attributed to C1TMS's rapid hydrolysis and high dispersion in water, which facilitated its adsorption onto particle surfaces. The adsorbed silane hindered the dissolution and migration of ions and suppressed the continuous deposition of hydration products, thereby significantly delaying the setting process [69]. C4TMS, C8TMS, and C12TMS increased the final setting time by 90.3%, 31.3%, and 14.0%, respectively. These alkyl silanes form hydrophobic coatings that inhibit water diffusion and particle wetting, partially suppressing hydration. However, with increasing chain length, poorer dispersion reduces their interference with hydration, thus lessening the retardation effect. The AAFS reference paste set much faster than OPC, with a final setting time of 2.16 h. Similarly, alkyl silanes also delayed AAFS paste setting, but to a much lesser extent than in OPC, and long-chain silanes showed minimal effects. C1TMS extended the final setting time to 3.95 h, as its hydrolyzed methylsilanol condensed with reactive Si–OH and Al–OH groups, forming localized cross-linked networks that occupied active sites and hindered the further dissolution and polymerization of reactive species, thereby delaying the formation of a continuous gel network. C4TMS increased the final setting time by 26.6%. In contrast, the retardation effects of C8TMS and C12TMS were negligible, extending the final setting time by only 9.3% and 5.6%, respectively. These results suggest that long-chain alkyl silanes exert limited interference with the setting of cementitious materials, whereas short-chain alkyl silanes can effectively serve as alternative retarders.
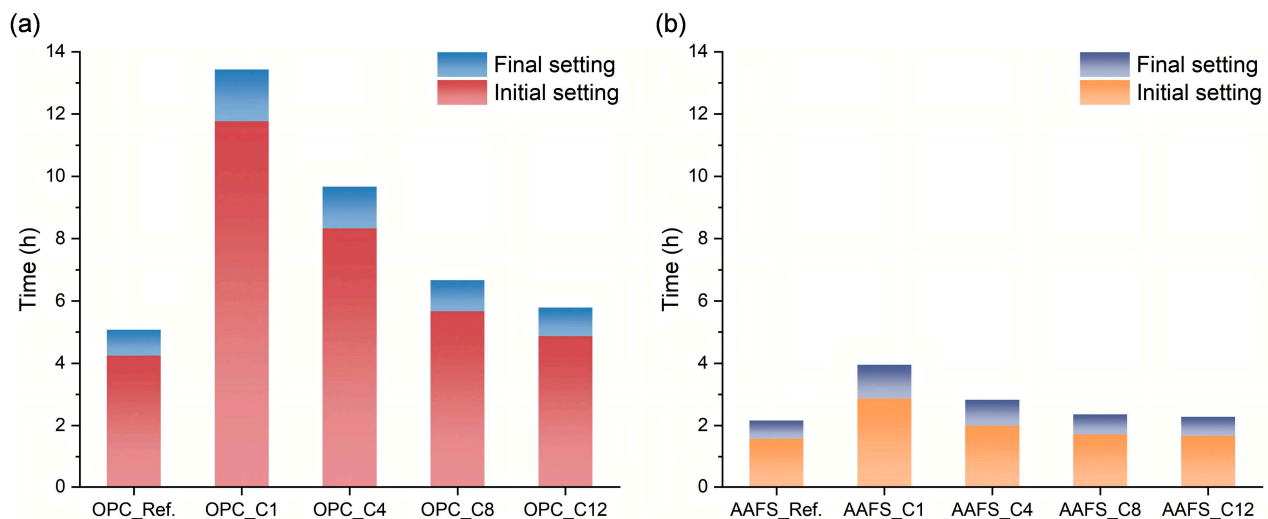
Figure 7. Initial and final setting times of (**a**) OPC and (**b**) AAFS pastes with 1% alkyl silanes.

3.4. Reaction Kinetics

Isothermal calorimetry was conducted to investigate the effects of 1% alkyl silane on the heat evolution rate and cumulative heat release of OPC and AAFS pastes over the first 88 h, as shown in Figure 8. The incorporation of alkyl silanes did not introduce or eliminate additional exothermic peaks but altered their intensity and occurrence time. Figure 8a presents the heat flow curves of OPC pastes with different alkyl silanes. All pastes exhibited three characteristic exothermic stages: (i) an initial instantaneous peak related to particle wetting and rapid ion dissolution within the first hour; (ii) the main exothermic peak corresponding to the formation of C–S–H gel and $Ca(OH)_2$ between approximately 10 and 50 h; and (iii) a late-stage slow exothermic phase reflecting the continued growth and densification of hydration products [72,73]. The main exothermic peak of the reference group occurred at about 20.3 h. Compared with the reference paste, C1TMS and C4TMS delayed the peak by approximately 10.7 h and 1.7 h, respectively, with C1TMS showing the most significant retardation. This is mainly attributed to the rapid hydrolysis and uniform adsorption of short-chain alkyl silanes on particle surfaces, restricting water and ion diffusion and thus suppressing early nucleation of hydration products [69]. In contrast, C8TMS and C12TMS advanced the main exothermic peak by approximately 3.8 h and 3.9 h, respectively, while exhibiting slightly lower peak intensities than the reference paste and an extended plateau stage. This could be explained by the formation of a hydrophobic enrichment layer by long-chain alkyl silanes, which locally increased ion concentration and accelerated surface hydration. However, hydration products were confined to local regions, slowing the formation of a continuous network and slightly prolonging the setting time. Additionally, gradual hydrolysis of long-chain alkyl silanes catalyzed by hydroxide ions released from cement particles, accompanied by exothermic condensation, may have slightly accelerated the hydration process [74]. The cumulative heat release of OPC pastes is shown in Figure 8b. C1TMS-modified paste exhibited a noticeable increase in heat evolution after 36 h, with its cumulative heat surpassing that of the reference paste after 72 h. This is likely because the initially uniform and well-dispersed alkyl silane film, although hindering the early nucleation and growth, gradually underwent condensation reactions over time, forming pores and microcracks, which re-exposed hydration interfaces and promoted continued hydration product growth and matrix densification. In contrast, the cumulative heat of C4TMS- and C8TMS-modified pastes remained below that of the reference paste after 72 h, while that of C12TMS was close to that of the reference paste but still slightly lower. This indicates that the hydrophobic layers formed by medium- and

long-chain silanes were more stable, providing insufficient reactive interfaces in the later stage and resulting in slower overall growth rates.
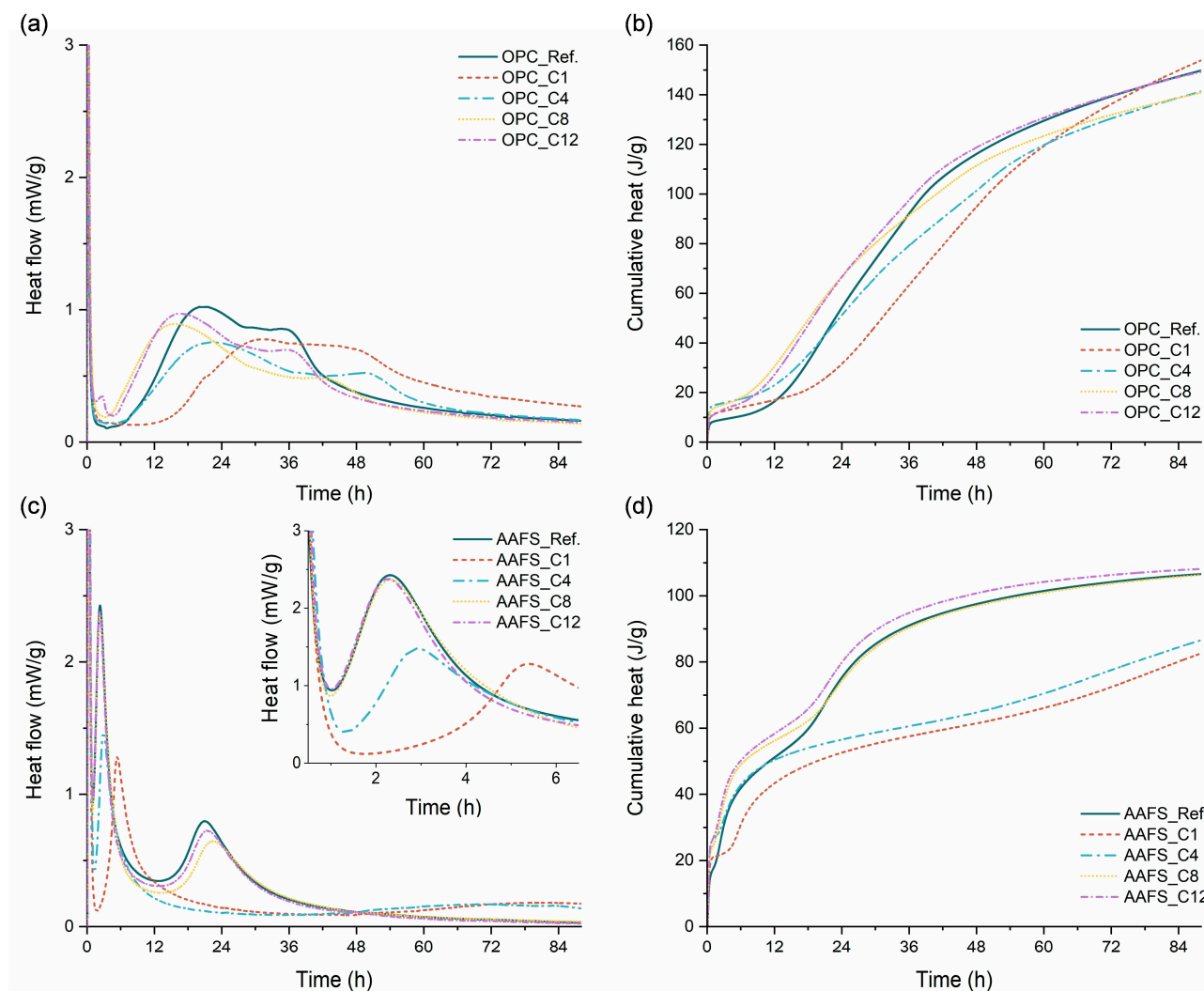

Figure 8. (**a,c**) Heat flow and (**b,d**) cumulative heat of (**a,b**) OPC and (**c,d**) AAFS pastes with 1% alkyl silane.

The heat flow curves of AAFS pastes are shown in Figure 8c. Three typical peaks were observed: (i) an initial sharp peak occurring within the first 0.5 h, corresponding to the rapid wetting and partial dissolution of FA and GGBS particles; (ii) a second peak centered around 2–6 h, associated with the early-stage reaction between soluble silicate species from the waterglass and calcium sources from GGBS; and (iii) a broad peak spanning from approximately 18 h to 88 h, attributed to continuous gel network formation and structural rearrangement [75–77]. For the reference paste, the second and third peaks occurred at approximately 2.3 h and 21.0 h, respectively. In comparison, C1TMS and C4TMS delayed the second peak by about 3.1 h and 0.7 h, and postponed the third peak by more than 40 h. Similarly to OPC, short-chain alkyl silanes rapidly hydrolyzed and condensed with active Si–OH and Al–OH sites in the highly alkaline environment, occupying reactive sites and hindering the dissolution and migration of reactive species, thereby prolonging the induction period. Relative to the reference paste, C8TMS and C12TMS had negligible influence on the second peak and only delayed the third peak by approximately 1.3 h and 0.4 h, respectively. The cumulative heat release of AAFS pastes (Figure 8d) also reflected these trends. C1TMS- and C4TMS-modified pastes showed much lower early cumulative

heat release than the reference but exhibited accelerated growth after 48 h, indicating a delayed yet promoting effect in the later stage. AAFS pastes with long-chain alkyl silanes showed cumulative heat release comparable to the reference, suggesting a limited overall effect on the reaction process. Early cumulative heat release is generally regarded as an indicator of the reaction degree [45]. These findings are consistent with the compressive strength results discussed below.

3.5. Compressive Strength

Figure 9a shows the compressive strength development of OPC pastes at 1, 3, 7, and 28 d, which corresponds closely to the reaction kinetics results. At 1 d, C1TMS and C4TMS significantly reduced the compressive strength by 35.7% and 14.8%, respectively, relative to the mean value of the reference paste, whereas C8TMS and C12TMS had minimal effects, even slightly increasing strength by 0.7–2.9%. This aligns with the delayed main exothermic peaks of C1TMS and C4TMS, indicating that short-chain alkyl silanes significantly inhibited early nucleation and structural development, while long-chain alkyl silanes exerted weaker suppression. At 3 and 7 d, C1TMS increased the compressive strength by 7.1% and 17.9%, respectively, owing to its retarding effect, which facilitated denser microstructure formation after hydration recovery [78]. Conversely, C4TMS reduced strength by 26.6% and 12.8%, while C8TMS and C12TMS decreased it by 10.3–16.4%. The stable hydrophobic layers formed by long-chain alkyl silanes continuously impeded hydration interfaces, limiting C–S–H filling of macropores and capillary pores, thereby producing a looser pore structure at later stages and reducing strength [49]. At 28 d, alkyl silanes decreased the compressive strength by 0.3–24.6%, with the extent of reduction increasing initially and then levelling off as the alkyl chain length increased.
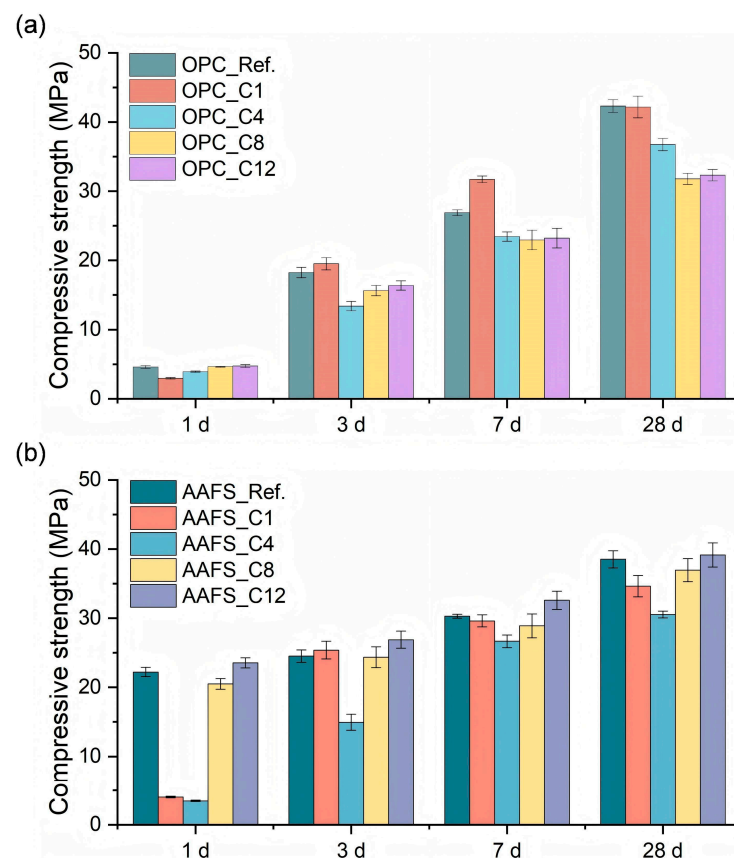

Figure 9. Compressive strength of (**a**) OPC and (**b**) AAFS pastes with 1% alkyl silanes cured for 1, 3, 7, and 28 d.

The compressive strength of AAFS pastes (Figure 9b) exhibited a different pattern compared to that of OPC pastes. The AAFS reference paste showed much higher early compressive strength than OPC, with 1-day strength approximately 4.8 times greater, demonstrating the early-strength advantage of alkali-activated materials [8,11]. C1TMS and C4TMS significantly delayed early strength development, reducing 1-day compressive strength by 82.0% and 84.5%, respectively. In contrast, long-chain alkyl silanes had negligible effects, with C12TMS even increasing strength slightly by 6.0%. This is also consistent with the calorimetry results, which showed that short-chain silanes markedly delayed the exothermic peak of AAFS paste, while longer-chain silanes had weaker effects, with C12TMS exhibiting a higher cumulative heat release than the reference paste. At 3 d, C1TMS-modified pastes exhibited rapid strength gain, while C4TMS-modified pastes, though still lower than the reference, recovered substantially compared to 1 d. As the reaction progressed, OH^- gradually penetrated the hydrophobic layers, accelerating Si and Al dissolution and promoting gel deposition. The uniform and stable hydrophobic film formed by C4TMS, owing to its good dispersibility, may have severely hindered the transport of reactive species and the formation of gels, leading to irreversible early pore defects and potentially contributing to the lowest strength [32]. With increasing chain length, the inhibitory effect of alkyl silanes on AAFS strength was weakened due to the reduced dispersibility. Moreover, the slight improvement in AAFS paste workability by long-chain alkyl silanes may have potentially optimized initial particle packing and refined the air-induced pore structure [79]. At 28 d, AAFS strength first decreased and then increased with increasing chain length.

3.6. Matrix Wettability

Figure 10 presents the WCA of the polished fracture surfaces of OPC and AAFS pastes. The incorporation of alkyl silanes markedly altered the wettability of both matrices, exhibiting a similar trend in both systems but with varying degrees of impact. For the OPC system, the reference paste showed a WCA of only 53°, indicating hydrophilicity. The WCA of the C1TMS-modified paste decreased to 20°, as its short alkyl chain provided weak hydrophobicity and failed to form an effective hydrophobic layer, while its rapid hydrolysis and high dispersion generated abundant hydrophilic Si–OH groups, further enhancing wettability [47]. In contrast, C4TMS, C8TMS, and C12TMS significantly improved surface hydrophobicity, with WCAs of 123°, 145°, and 116°, respectively, among which C8TMS exhibited the best performance. Its chain length allowed relatively uniform adsorption on hydration products, forming a hydrophobic film with the best hydrophobic effect. C4TMS, despite its good dispersion, exhibited slightly weaker hydrophobicity than C8TMS, while C12TMS showed reduced effectiveness due to poor dispersion and the formation of discontinuous hydrophobic coverage caused by rapid self-condensation and aggregation. The AAFS reference paste exhibited even stronger hydrophilicity, with a WCA of only 19°, likely due to its higher content of surface hydroxyl groups. The addition of C1TMS further reduced its hydrophobicity for reasons similar to those in OPC. C4TMS achieved the highest hydrophobic enhancement, raising the WCA to 150°, which can be attributed to its moderate hydrolysis rate and good dispersion in the highly alkaline environment, enabling the formation of a uniform siloxane network with abundant exposed hydrophobic alkyl groups. The WCAs of C8TMS- and C12TMS-modified AAFS pastes increased to 134° and 77°, respectively, showing a declining trend in hydrophobicity with increasing chain length. This may be attributed to the higher susceptibility of long-chain silanes to hydrolysis under high alkalinity. In addition, their strong intrinsic hydrophobicity promotes the self-condensation and localized aggregation of silanes, which markedly reduce their dispersion in the paste and leave a large proportion of hydrophilic groups in the matrix

unmodified [51]. These findings indicate that the hydrophobic effect does not simply increase with chain length but results from a balance between intrinsic hydrophobicity and dispersion uniformity. In subsequent applications, silanes with appropriate chain lengths can be selected according to the matrix type and the required waterproof performance to achieve optimal modification.
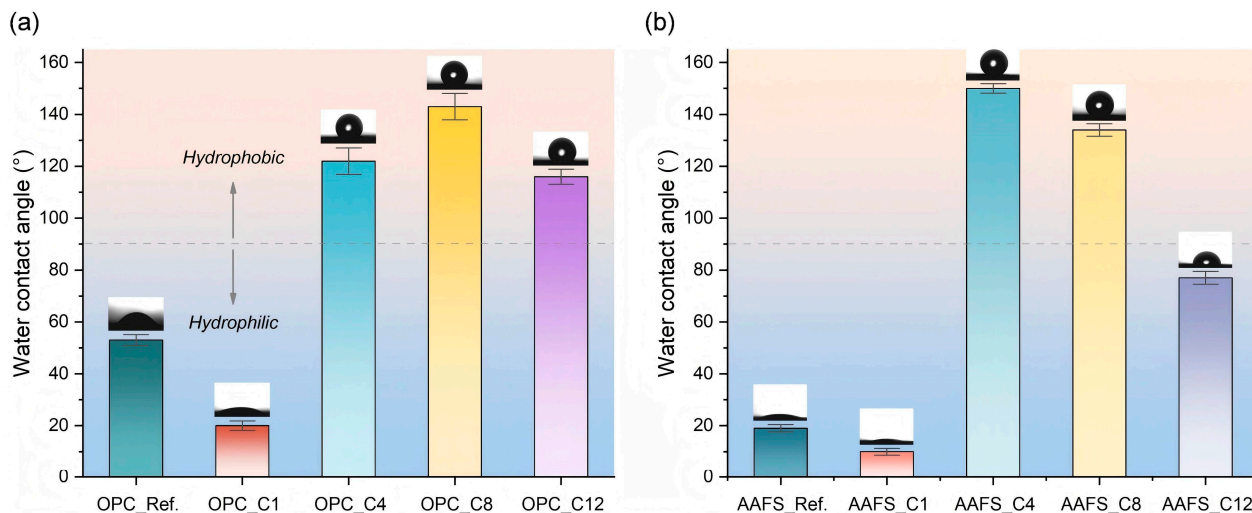

Figure 10. WCA of the polished fracture surface of (**a**) OPC and (**b**) AAFS pastes with 1% alkyl silanes.

3.7. Water Absorption Behavior

To evaluate the effect of alkyl silanes on the water resistance of OPC and AAFS, water absorption tests were performed on pastes with 1% alkyl silanes of different chain lengths, as shown in Figure 11. The percentage water absorption was calculated as the ratio of the absorbed water mass to the initial specimen mass. All OPC pastes exhibited water uptake following the Hall model, with water absorption proportional to the square root of time within the first 20 h [80]. The slope of this initial linear stage, defined as the water sorptivity, reflects the rate of water and harmful substance ingress and is a critical indicator of concrete durability [41]. The AAFS reference paste exhibited rapid water uptake within the first 1 h, showing a linear relationship with the square root of time, after which the slope gradually decreased, consistent with previous findings [18,45]. This indicates that AAFS paste is more hydrophilic than OPC paste, which aligns with the WCA results. Therefore, to accurately reflect the initial water transport characteristics, the water sorptivity was calculated based on the first 20 h of water absorption for OPC paste and the first 1 h for AAFS paste, as shown in Figure 12 and Table 5. C1TMS significantly increased the water sorptivity of the OPC paste by 77.7%, indicating enhanced hydrophilicity. In contrast, C4TMS and C8TMS effectively reduced water sorptivity by around 75% ± 0.7%, whereas C12TMS showed weaker sorptivity suppression of 39.2%. A similar trend was observed in AAFS pastes. C1TMS increased water sorptivity by 8.6%, while C4TMS, C8TMS, and C12TMS all markedly reduced it. Due to the inherently high absorption rate of AAFS paste, the same silane dose produced a more pronounced reduction compared to OPC paste, with C4TMS achieving the best water resistance (a 97.0% decrease), followed by C8TMS (95.7%) and C12TMS (84.4%). For both OPC and AAFS pastes, wettability and water transport behavior exhibited strong correlation: higher WCA corresponded to lower water sorptivity. As reported, capillary absorption in porous cementitious materials is mainly governed by pore structure and the interfacial properties of water, including the surface energy, dynamic viscosity and solid–liquid–gas contact angle [41]. Given that the surface energy and dynamic viscosity of water are negligible, the wettability of the matrix

is a key factor influencing water transport in alkyl silane-modified OPC and AAFS pastes, consistent with previous studies [81,82].
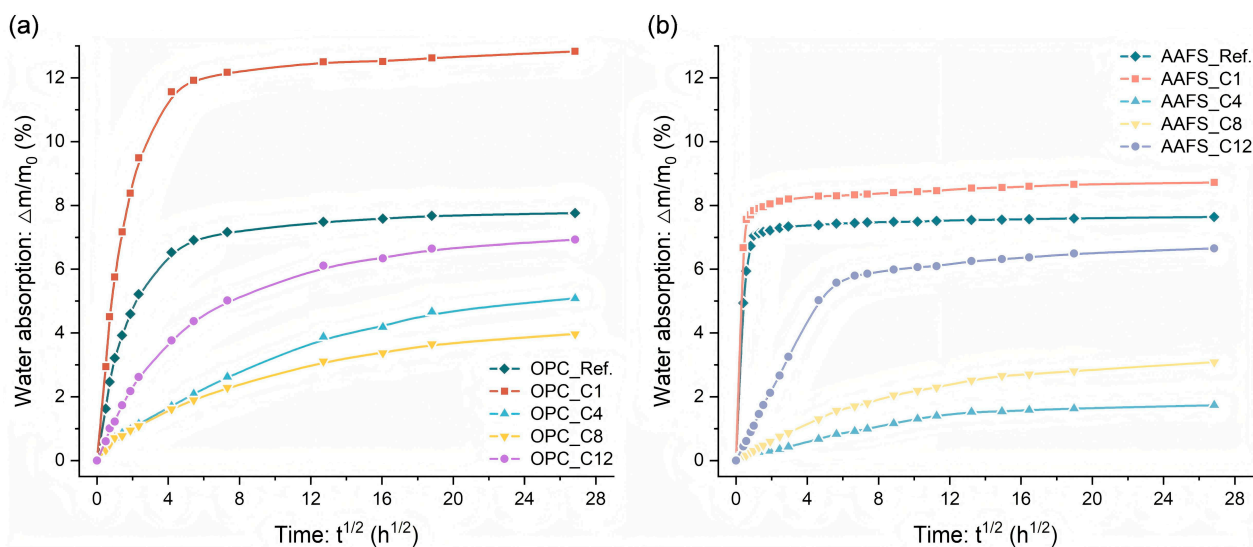

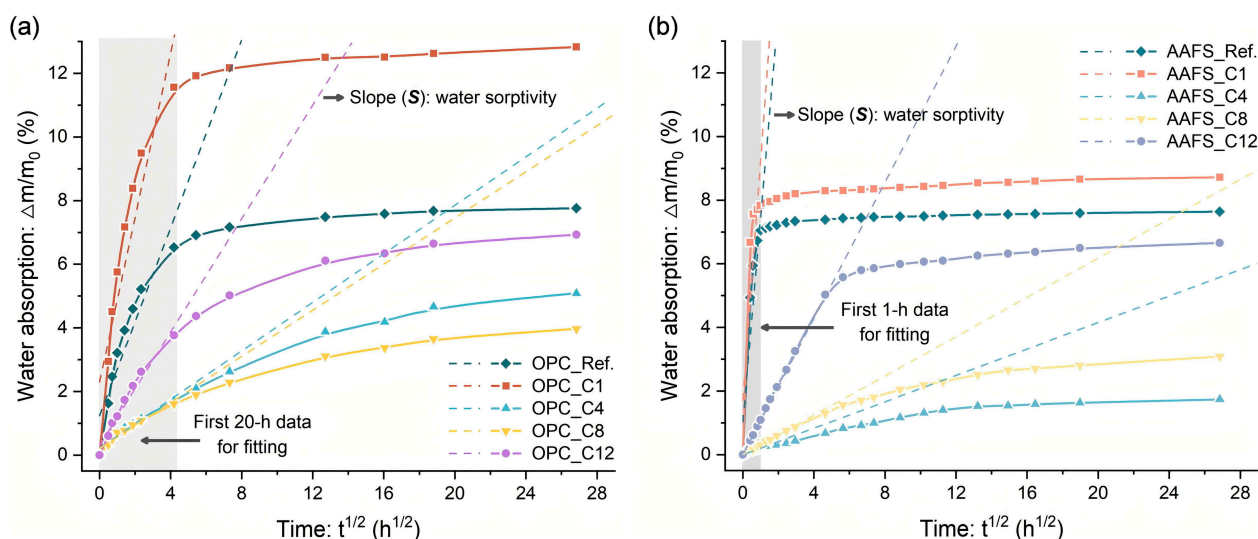**Figure 11.** Water absorption process of (**a**) OPC and (**b**) AAFS pastes with 1% alkyl silanes.

Figure 12. Schematic diagram of calculating water sorptivity from linear fit of the initial water absorption data: (**a**) OPC (first 20 h) and (**b**) AAFS (first 1 h).

Table 5. Water sorptivity results for OPC and AAFS pastes with 1% alkyl silanes.

Mixture	Water Sorptivity	Mixture	Water Sorptivity
OPC_Ref.	1.48	AAFS_Ref.	6.99
OPC_C1	2.63	AAFS_C1	7.59
OPC_C4	0.38	AAFS_C4	0.21
OPC_C8	0.36	AAFS_C8	0.30
OPC_C12	0.90	AAFS_C12	1.09

4. Conclusions

This study systematically investigated the effects of silanes with different alkyl chain lengths, i.e., C1TMS, C4TMS, C8TMS, and C12TMS, on the early-age properties and reaction of OPC and AAFS pastes. The work focused on rheology, fluidity, setting behavior, reac-

tion kinetics, compressive strength, and hydrophobic modification effects. The following conclusions can be drawn:

- The effects of alkyl silanes on the paste rheology and flowability were affected by both alkyl chain length of silanes and binder systems. In OPC, C1TMS reduced the yield stress and plastic viscosity by 33.6% and 21.0%, respectively, and enhanced flowability by 27.6%. However, C4TMS, C8TMS, and C12TMS showed the opposite effect compared to C1TMS due to improved hydrophobicity, with 54.2–314.6% increase in yield stress and 11.0–70.0% in plastic viscosity. In contrast, the plastic viscosity of AAFS just changed within 5.2–13.1% due to alkyl silane incorporation. Additionally, although AAFS pastes showed higher plastic viscosity than OPC, its lower yield stress and the "ball-bearing" effect of FA particles contributed to superior flowability.

- All alkyl silanes delayed setting of OPC and AAFS pastes, with shorter chains causing stronger retardation. C1TMS and C4TMS postponed the main exothermic peaks of both binder systems and suppressed early gel formation but promoted reaction recovery at later stages. C8TMS and C12TMS had relatively minor effects on the setting time and the early heat release.

- Compressive strength development correlated well with early-age reaction kinetics. AAFS pastes showed higher 1-day strength than OPC. C1TMS and C4TMS suppressed early strength development, reducing the 1-day strength of OPC by 14.8–35.7% and AAFS by 82.0–84.5%. However, C1TMS-modified OPC and AAFS pastes showed accelerated strength development after 3 d.

- Hydrophobic performance was mainly governed by alkyl chain length and dispersion uniformity of silanes. In OPC, C8TMS showed the best hydrophobic modification effect, yielding a WCA of 145° and reducing water sorptivity by 75.7%. C4TMS and C12TMS also improved hydrophobicity. C1TMS, with limited hydrophobic methyl groups and abundant hydrophilic Si–OH, increased water sorptivity and decreased WCA. Similar trends were observed in AAFS pastes, with C4TMS showing the best hydrophobicity, followed by C8TMS and C12TMS.

Overall, this study provides valuable insights for designing water-resistant cementitious materials across different systems and application scenarios. The findings indicate that C1TMS, though ineffective for improving water resistance, can function as a retarder or workability modifier for pumped or mass concrete due to its viscosity-reducing and set-delaying effects. C4TMS and C8TMS are promising integral hydrophobic modifiers, with C8TMS favored for OPC and C4TMS for AAFS. C12TMS, despite strong inherent hydrophobicity but poorer dispersion, is more suitable for applications requiring primarily surface hydrophobicity. The combination of high viscosity and minimal setting delay observed for C8TMS and C12TMS in OPC suggests their potential as modifiers for low-flow, rapid-application waterproof coatings or protective layers. This work was conducted at a fixed silane dose (1%) and primarily focused on the early-age properties. In future research, systematic investigations will be conducted on varying doses, long-term durability, and microstructural evolution, together with broader application scenarios, to further elucidate the organic–inorganic hybridization mechanisms, performance characteristics, and engineering potential of such modified systems.

Author Contributions: Conceptualization, R.G. and S.R.; Methodology, R.G., J.M. and W.T.; Formal analysis, R.G. and W.T.; Investigation, R.G. and J.M.; Resources, D.Y.; Data curation, R.G., J.M. and Y.W.; Writing—original draft, R.G.; Writing—review & editing, R.G., S.R. and D.Y.; Visualization, R.G., W.T. and Y.W.; Supervision, S.R.; Funding acquisition, D.Y. All authors have read and agreed to the published version of the manuscript.

Data Availability Statement: The original contributions presented in the study are included in the article, further inquiries can be directed to the corresponding author.

Conflicts of Interest: The authors declare no conflicts of interest.

References

1. Monteiro, P.J.; Miller, S.A.; Horvath, A. Towards Sustainable Concrete. *Nat. Mater.* **2017**, *16*, 698–699. [CrossRef]
2. Habert, G.; Miller, S.A.; John, V.M.; Provis, J.L.; Favier, A.; Horvath, A.; Scrivener, K.L. Environmental Impacts and Decarbonization Strategies in the Cement and Concrete Industries. *Nat. Rev. Earth Environ.* **2020**, *1*, 559–573. [CrossRef]
3. Provis, J.L.; Palomo, A.; Shi, C. Advances in Understanding Alkali-Activated Materials. *Cem. Concr. Res.* **2015**, *78*, 110–125. [CrossRef]
4. Shi, C.; Qu, B.; Provis, J.L. Recent Progress in Low-Carbon Binders. *Cem. Concr. Res.* **2019**, *122*, 227–250. [CrossRef]
5. Provis, J.L. Alkali-Activated Materials. *Cem. Concr. Res.* **2018**, *114*, 40–48. [CrossRef]
6. Jiang, C.; Wang, A.; Bao, X.; Ni, T.; Ling, J. A Review on Geopolymer in Potential Coating Application: Materials, Preparation and Basic Properties. *J. Build. Eng.* **2020**, *32*, 101734. [CrossRef]
7. Amran, Y.M.; Alyousef, R.; Alabduljabbar, H.; El-Zeadani, M. Clean Production and Properties of Geopolymer Concrete; A Review. *J. Clean. Prod.* **2020**, *251*, 119679. [CrossRef]
8. Zhu, H.; Ren, J. Effects of Nano-SiO$_2$ and Mixing Water on Early-Strength Mechanisms of High-Fluidity Slag and Desulfurization Gypsum Composite Alkali Activated Materials. *Constr. Build. Mater.* **2025**, *492*, 142959. [CrossRef]
9. Luo, Y.; Li, S.; Klima, K.; Brouwers, H.; Yu, Q. Degradation Mechanism of Hybrid Fly Ash/Slag Based Geopolymers Exposed to Elevated Temperatures. *Cem. Concr. Res.* **2022**, *151*, 106649. [CrossRef]
10. Hojati, M.; Radlińska, A. Shrinkage and Strength Development of Alkali-Activated Fly Ash-Slag Binary Cements. *Constr. Build. Mater.* **2017**, *150*, 808–816. [CrossRef]
11. Zhang, P.; Wang, K.; Li, Q.; Wang, J.; Ling, Y. Fabrication and Engineering Properties of Concretes Based on Geopolymers/Alkali-Activated Binders-A Review. *J. Clean. Prod.* **2020**, *258*, 120896. [CrossRef]
12. Shen, C.; Zhu, Y.; Shi, W.; He, K.; Xiao, X.; Xu, X.; Shi, J.; Xu, G. Mechanically Stable Superhydrophobic Surface on Cement-Based Materials. *Chem. Phys.* **2020**, *538*, 110912. [CrossRef]
13. Zhang, D.; Zhu, H.; Wu, Q.; Yang, T.; Yin, Z.; Tian, L. Investigation of the Hydrophobicity and Microstructure of Fly Ash-Slag Geopolymer Modified by Polydimethylsiloxane. *Constr. Build. Mater.* **2023**, *369*, 130540. [CrossRef]
14. Jiang, C.; Jiang, L.; Li, S.; Tang, X.; Zhang, L. Impact of Cation Type and Fly Ash on Deterioration Process of High Belite Cement Pastes Exposed to Sulfate Attack. *Constr. Build. Mater.* **2021**, *286*, 122961. [CrossRef]
15. Peng, Y.; Zhao, G.; Qi, Y.; Zeng, Q. In-Situ Assessment of the Water-Penetration Resistance of Polymer Modified Cement Mortars by μ-XCT, SEM and EDS. *Cem. Concr. Compos.* **2020**, *114*, 103821. [CrossRef]
16. Wen, J.; Wan, Y.; Xu, C.; Yang, Y. A Review of New Methods for Measuring Saturation of Concrete and Its Impact on Concrete Properties. *J. Build. Eng.* **2024**, *96*, 110664. [CrossRef]
17. Yi, Y.; Zhu, D.; Guo, S.; Zhang, Z.; Shi, C. A Review on the Deterioration and Approaches to Enhance the Durability of Concrete in the Marine Environment. *Cem. Concr. Compos.* **2020**, *113*, 103695. [CrossRef]
18. Li, Q.; Yang, K.; Yang, C. An Alternative Admixture to Reduce Sorptivity of Alkali-Activated Slag Cement by Optimising Pore Structure and Introducing Hydrophobic Film. *Cem. Concr. Compos.* **2019**, *95*, 183–192. [CrossRef]
19. Liang, G.; Liu, T.; Li, H.; Wu, K. Shrinkage Mitigation, Strength Enhancement and Microstructure Improvement of Alkali-Activated Slag/Fly Ash Binders by Ultrafine Waste Concrete Powder. Compos. *Part B Eng.* **2022**, *231*, 109570. [CrossRef]
20. Li, H.; Guo, X. Fabricating Hydrophobic Silica Fume to Improve Mechanical Strength and Anti-Corrosion of Integral Hydrophobic Cement Mortar and Its Carbon Emission Assessment. *J. Clean. Prod.* **2024**, *439*, 140857. [CrossRef]
21. Sidhu, J.; Kumar, P. Development of Hydrophobicity in Geopolymer Composites-Progress and Perspectives. *Constr. Build. Mater.* **2023**, *396*, 132344. [CrossRef]
22. Wu, B.; Qiu, J. Enhancing the Hydrophobic PP Fiber/Cement Matrix Interface by Coating Nano-AlOOH to the Fiber Surface in a Facile Method. *Cem. Concr. Compos.* **2022**, *125*, 104297. [CrossRef]
23. Manabe, K.; Saikawa, M.; Sato, I.; Loo, C.S.; Takashima, K.; Norikane, Y. Biomimetic 3D-Printed Armored Structures for Durable Superhydrophobic Surfaces: Integrating Macroprotection and Nanofunctionality. *ACS Appl. Polym. Mater.* **2024**, *6*, 13701–13709. [CrossRef]

24. Ruan, S.; Chen, S.; Liu, Y.; Yan, D.; Sun, Z. Investigation on the Effect of Fiber Wettability on Water Absorption Kinetics of Geopolymer Composites. *Ceram. Int.* **2022**, *48*, 36678–36689. [CrossRef]

25. Sánchez, R.Z.; Gonzalez-Coneo, J.; Luna, M.; Diaz, A.; Mosquera, M.J. Studying the Bulk Hydrophobization of Cement Mortars by the Combination of Alkylalkoxysilane Admixture and Fluoropolymer-Functionalized Aggregate. *J. Build. Eng.* **2023**, *65*, 105771. [CrossRef]

26. Wang, F.; Lei, S.; Ou, J.; Li, W. Effect of PDMS on the Waterproofing Performance and Corrosion Resistance of Cement Mortar. *Appl. Surf. Sci.* **2020**, *507*, 145016. [CrossRef]

27. Muzenski, S.; Flores-Vivian, I.; Sobolev, K. Hydrophobic Engineered Cementitious Composites for Highway Applications. *Cem. Concr. Compos.* **2015**, *57*, 68–74. [CrossRef]

28. Wen, J.; Wan, Y.; Yang, Y. Sustainable Synthesis of Hydrophobic Waste Glass Powder for Enhanced Water and Frost Resistance in Mortar. *Constr. Build. Mater.* **2025**, *487*, 142097. [CrossRef]

29. Yao, H.; Xie, Z.; Huang, C.; Yuan, Q.; Yu, Z. Recent Progress of Hydrophobic Cement-Based Materials: Preparation, Characterization and Properties. *Constr. Build. Mater.* **2021**, *299*, 124255. [CrossRef]

30. Shen, Y.; Wu, Y.; Shen, Z.; Chen, H. Fabrication of Self-Healing Superhydrophobic Surfaces from Water-Soluble Polymer Suspensions Free of Inorganic Particles through Polymer Thermal Reconstruction. *Coatings* **2018**, *8*, 144. [CrossRef]

31. Gao, R.; Mao, J.; Ruan, S.; Qiu, Y.; Ye, S.; Chen, S.; Liu, Y.; Yan, D. A Comparative Study of Metakaolin-Based Geopolymers with Immobilised Organic Liquids: Vegetable Oil, Mineral Oil, and Organosilicon Liquids. *J. Build. Eng.* **2025**, *108*, 112860. [CrossRef]

32. Feng, B.; Liu, J.; Chen, Y.; Tan, X.; Zhang, M.; Sun, Z. Properties and Microstructure of Self-Waterproof Metakaolin Geopolymer with Silane Coupling Agents. *Constr. Build. Mater.* **2022**, *342*, 128045. [CrossRef]

33. John, S.K.; Nadir, Y.; Cascardi, A.; Arif, M.M.; Girija, K. Effect of Addition of Nanoclay and SBR Latex on Fly Ash-Slag Geopolymer Mortar. *J. Build. Eng.* **2023**, *66*, 105875. [CrossRef]

34. Zhang, J.; Xiao, M.; Feng, Y. A Review on Nanomaterials and Polymers Modified Cementitious Materials with High Performances. *J. Build. Eng.* **2025**, *104*, 112331. [CrossRef]

35. Di Mundo, R.; Labianca, C.; Carbone, G.; Notarnicola, M. Recent Advances in Hydrophobic and Icephobic Surface Treatments of Concrete. *Coatings* **2020**, *10*, 449. [CrossRef]

36. Zhao, J.; Gao, X.; Chen, S.; Lin, H.; Li, Z.; Lin, X. Hydrophobic or Superhydrophobic Modification of Cement-Based Materials: A Systematic Review. *Compos. Part B Eng.* **2022**, *243*, 110104. [CrossRef]

37. Sandrolini, F.; Franzoni, E.; Pigino, B. Ethyl Silicate for Surface Treatment of Concrete–Part I: Pozzolanic Effect of Ethyl Silicate. *Cem. Concr. Compos.* **2012**, *34*, 306–312. [CrossRef]

38. Ruan, S.; Gao, R.; Tu, W.; Li, G.; Lu, J.-X.; Yan, D.; Poon, C.S. Hydration Products and Hybridisation Mechanisms of Hydrophobic Cement Pastes with Alkyl-Organosilanes. *Cem. Concr. Compos.* **2025**, *163*, 106208. [CrossRef]

39. Pape, P.G. Silane Coupling Agents: Enhancements of Physical Properties of Plastics. *Eng. Plast.* **1996**, *9*, 109–115.

40. Otte, M.; Schweinitz, A.; Bonus, M.; Enke, U.; Schumann, C.; Gohlke, H.; Benndorf, K. Hydrophobic Alkyl Chains Substituted to the 8-Position of Cyclic Nucleotides Enhance Activation of CNG and HCN Channels by an Intricate Enthalpy-Entropy Compensation. *Sci. Rep.* **2018**, *8*, 14960. [CrossRef]

41. Zhang, C.; Zhang, S.; Yu, J.; Kong, X. Water Absorption Behavior of Hydrophobized Concrete Using Silane Emulsion as Admixture. *Cem. Concr. Res.* **2022**, *154*, 106738. [CrossRef]

42. She, W.; Zheng, Z.; Zhang, Q.; Zuo, W.; Yang, J.; Zhang, Y.; Zheng, L.; Hong, J.; Miao, C. Predesigning Matrix-Directed Super-Hydrophobization and Hierarchical Strengthening of Cement Foam. *Cem. Concr. Res.* **2020**, *131*, 106029. [CrossRef]

43. Wang, D.; Wu, X.; Yuan, L.; Wu, D.; Zhao, Q.; Pan, H.; Qi, W. Oil Absorption and Plant Symbiosis Capacity of Hydrophobic Modified Concrete: Preparation and Performance Analysis. *Constr. Build. Mater.* **2024**, *413*, 134897. [CrossRef]

44. Li, F.; Liu, L.; Liu, K.; Zheng, A.; Liu, J. Investigation on Waterproof Mechanism and Micro-Structure of Cement Mortar Incorporated with Silicane. *Constr. Build. Mater.* **2020**, *239*, 117865. [CrossRef]

45. She, Y.; Chen, Y.; Li, L.; Xue, L.; Yu, Q. Understanding the Generation and Evolution of Hydrophobicity of Silane Modified Fly Ash/Slag Based Geopolymers. *Cem. Concr. Compos.* **2023**, *142*, 105206. [CrossRef]

46. Yang, J.; Zuo, W.; She, W. Towards a Further Understanding of Cement Hydration at the Early-Age Stage in the Presence of Hydrophobic Silane IBTEO. *Cem. Concr. Compos.* **2024**, *153*, 105712. [CrossRef]

47. Koohestani, B. Effect of Saline Admixtures on Mechanical and Microstructural Properties of Cementitious Matrices Containing Tailings. *Constr. Build. Mater.* **2017**, *156*, 1019–1027. [CrossRef]

48. Chen, B.; Shao, H.; Li, B.; Li, Z. Influence of Silane on Hydration Characteristics and Mechanical Properties of Cement Paste. *Cem. Concr. Compos.* **2020**, *113*, 103743. [CrossRef]

49. Xie, M.; Zhong, Y.; Li, Z.; Lei, F.; Jiang, Z. Study on Alkylsilane-Incorporated Cement Composites: Hydration Mechanism and Mechanical Properties Effects. *Cem. Concr. Compos.* **2021**, *122*, 104161. [CrossRef]

50. Verma, C.; Quraishi, M.; Rhee, K. Hydrophilicity and Hydrophobicity Consideration of Organic Surfactant Compounds: Effect of Alkyl Chain Length on Corrosion Protection. *Adv. Colloid Interface Sci.* **2022**, *306*, 102723. [CrossRef]

51. Zhao, H.; Yang, Y.; Shu, X.; Dong, L.; Qiao, M.; Ran, Q. Micelle Conformation of Sodium Alkyl Sulfate Surfactants with Different Hydrophobic Chain Length: A Molecular Dynamics Study. *Comput. Mater. Sci.* **2023**, *229*, 112452. [CrossRef]

52. Ruan, S.; Gao, R.; Tu, W.; Yan, D.; Zhang, M. Alkali-Activated Materials with Organics: A Critical Review. *Compos. Part B Eng.* **2024**, *284*, 111712. [CrossRef]

53. Dong, D.; Huang, Y.; Pei, Y.; Zhang, X.; Cui, N.; Zhao, P.; Hou, P.; Lu, L. Effect of Spherical Silica Fume and Fly Ash on the Rheological Property, Fluidity, Setting Time, Compressive Strength, Water Resistance and Drying Shrinkage of Magnesium Ammonium Phosphate Cement. *J. Build. Eng.* **2023**, *63*, 105484. [CrossRef]

54. Dai, X.; Aydin, S.; Yardimci, M.Y.; Qiang, R.; Lesage, K.; De Schutter, G. Rheology, Early-Age Hydration and Microstructure of Alkali-Activated GGBFS-Fly Ash-Limestone Mixtures. *Cem. Concr. Compos.* **2021**, *124*, 104244. [CrossRef]

55. Liu, Y.; Lu, C.; Hu, X.; Shi, C. Effect of Silica Fume on Rheology of Slag-Fly Ash-Silica Fume-Based Geopolymer Pastes with Different Activators. *Cem. Concr. Res.* **2023**, *174*, 107336. [CrossRef]

56. Sun, Y.; Zhang, S.; Rahul, A.; Tao, Y.; Van Bockstaele, F.; Dewettinck, K.; Ye, G.; De Schutter, G. Rheology of Alkali-Activated Slag Pastes: New Insight from Microstructural Investigations by Cryo-SEM. *Cem. Concr. Res.* **2022**, *157*, 106806. [CrossRef]

57. *GB/T 8077 2023*; Methods for Testing Uniformity of Concrete Admixtures. Standardization Administration of the People's Republic of China: Beijing, China, 2023.

58. Duan, K.; Wang, J.; Liu, Z.; Li, X.; Zhang, J.; Wang, X.; Wang, D. Flowability and In-Situ Phase Evolution of Na2CO3-Carbide Slag-Activated Blast Furnace Slag and Fly Ash. *Constr. Build. Mater.* **2025**, *466*, 140341. [CrossRef]

59. *GB/T 1346 2024*; Test Methods for Water Requirement of Normal Consistency, Setting Time and Soundness of the Port-land Cement. Standardization Administration of the People's Republic of China: Beijing, China, 2024.

60. *GB/T 17671-2021*; Method of Testing Cements—Determination of Strength (ISO Method). Standardization Administration of the People's Republic of China: Beijing, China, 2021.

61. Hisakado, T. Effect of Surface Roughness on Contact between Solid Surfaces. *Wear* **1974**, *28*, 217–234. [CrossRef]

62. *ASTM C642-13*; Standard Test Method for Density, Absorption, and Voids in Hardened Concrete. ASTM International: West Conshohocken, PA, USA, 2013.

63. Hall, C. Capillary Imbibition in Cement-Based Materials with Time-Dependent Permeability. *Cem. Concr. Res.* **2019**, *124*, 105835. [CrossRef]

64. Yang, T.; Zhu, H.; Zhang, Z.; Gao, X.; Zhang, C.; Wu, Q. Effect of Fly Ash Microsphere on the Rheology and Microstructure of Alkali-Activated Fly Ash/Slag Pastes. *Cem. Concr. Res.* **2018**, *109*, 198–207. [CrossRef]

65. Alnahhal, M.F.; Kim, T.; Hajimohammadi, A. Distinctive Rheological and Temporal Viscoelastic Behaviour of Alkali-Activated Fly Ash/Slag Pastes: A Comparative Study with Cement Paste. *Cem. Concr. Res.* **2021**, *144*, 106441. [CrossRef]

66. Li, L.; Wei, Y.; Li, Z.; Farooqi, M.U. Rheological and Viscoelastic Characterizations of Fly Ash/Slag/Silica Fume-Based Geopolymer. *J. Clean. Prod.* **2022**, *354*, 131629. [CrossRef]

67. Roussel, N.; Lemaître, A.; Flatt, R.J.; Coussot, P. Steady State Flow of Cement Suspensions: A Micromechanical State of the Art. *Cem. Concr. Res.* **2010**, *40*, 77–84. [CrossRef]

68. Favier, A.; Hot, J.; Habert, G.; de Lacaillerie, J.; Roussel, N. Rheology of Geopolymer: Comparative Study Between Portland Cement and Metakaolin Based Geopolymer. In *1st RILEM International Conference on Rheology and Processing of Construction Materials*; RILEM Publications Sarl: Paris, France, 2013; pp. 49–56.

69. Chen, B.; Wang, M.; Manzano, H.; Zhao, Y.; Li, Y. Molecular Elucidation of Cement Hydration Inhibition by Silane Coupling Agents. *Nat. Commun.* **2025**, *16*, 1597. [CrossRef]

70. Deb, P.S.; Nath, P.; Sarker, P.K. The Effects of Ground Granulated Blast-Furnace Slag Blending with Fly Ash and Activator Content on the Workability and Strength Properties of Geopolymer Concrete Cured at Ambient Temperature. *Mater. Des.* **2014**, *62*, 32–39. [CrossRef]

71. Pan, Z.; Tan, M.; Zheng, G.; Wei, L.; Tao, Z.; Hao, Y. Effect of Silica Fume Type on Rheology and Compressive Strength of Geopolymer Mortar. *Constr. Build. Mater.* **2024**, *430*, 136488. [CrossRef]

72. Lu, Z.; Kong, X.; Jansen, D.; Zhang, C.; Wang, J.; Pang, X.; Yin, J. Towards a Further Understanding of Cement Hydration in the Presence of Triethanolamine. *Cem. Concr. Res.* **2020**, *132*, 106041. [CrossRef]

73. Peng, L.; Jiang, Y.; Ban, J.; Shen, Y.; Ma, Z.; Zhao, Y.; Shen, P.; Poon, C.-S. Mechanism Underlying Early Hydration Kinetics of Carbonated Recycled Concrete Fines-Ordinary Portland Cement (CRCF-OPC) Paste. *Cem. Concr. Compos.* **2023**, *144*, 105275. [CrossRef]

74. Saeed, S.; Al Soubaihi, R.M.; White, L.S.; Bertino, M.F.; Saoud, K.M. Rapid Fabrication of Cross-Linked Silica Aerogel by Laser Induced Gelation. *Microporous Mesoporous Mater.* **2016**, *221*, 245–252. [CrossRef]

75. Gao, X.; Yu, Q.; Lazaro, A.; Brouwers, H. Investigation on a Green Olivine Nano-Silica Source Based Activator in Alkali Activated Slag-Fly Ash Blends: Reaction Kinetics, Gel Structure and Carbon Footprint. *Cem. Concr. Res.* **2017**, *100*, 129–139. [CrossRef]

76. Brough, A.; Atkinson, A. Sodium Silicate-Based, Alkali-Activated Slag Mortars: Part I. Strength, Hydration and Microstructure. *Cem. Concr. Res.* **2002**, *32*, 865–879. [CrossRef]

77. Zuo, Y.; Nedeljković, M.; Ye, G. Coupled Thermodynamic Modelling and Experimental Study of Sodium Hydroxide Activated Slag. *Constr. Build. Mater.* **2018**, *188*, 262–279. [CrossRef]

78. Barberena-Fernández, A.; Carmona-Quiroga, P.; Blanco-Varela, M.T. Interaction of TEOS with Cementitious Materials: Chemical and Physical Effects. *Cem. Concr. Compos.* **2015**, *55*, 145–152. [CrossRef]

79. Li, F.; Chen, Q.; Lu, Y.; Zou, Y.; Li, S. Dry Shrinkage and Micro-Structure of Alkali-Activated Fly Ash/Slag Pastes Incorporated with Silane Coupling Agent Modified MWCNTs. *Cem. Concr. Res.* **2024**, *175*, 107382. [CrossRef]

80. Kubissa, W.; Jaskulski, R. Measuring and Time Variability of the Sorptivity of Concrete. *Procedia Eng.* **2013**, *57*, 634–641. [CrossRef]

81. Ruan, S.; Yan, D.; Chen, S.; Jiang, F.; Shi, W. Process and Mechanisms of Multi-Stage Water Sorptivity in Hydrophobic Geopolymers Incorporating Polydimethylsiloxane. *Cem. Concr. Compos.* **2022**, *128*, 104460. [CrossRef]

82. Qu, Z.; Yu, Q.; Ji, Y.; Gauvin, F.; Voets, I.K. Mitigating Shrinkage of Alkali Activated Slag with Biofilm. *Cem. Concr. Res.* **2020**, *138*, 106234. [CrossRef]